An NADPH-oxidase/Polyamine Oxidase Feedback Loop Controls Oxidative Burst Under Salinity in tobacco

Article *in* Plant physiology · September 2016

DOI: 10.1104/pp.16.01118

8 authors, including:

Efthimios Andronis
University of Crete
9 PUBLICATIONS **62** CITATIONS
SEE PROFILE

Andreas Roussis
National and Kapodistrian University of Athens
36 PUBLICATIONS **985** CITATIONS
SEE PROFILE

Kalliopi Roubelakis-Angelakis
University of Crete
167 PUBLICATIONS **4,283** CITATIONS
SEE PROFILE

Running head: A PAO/NADPH-oxidase nexus

To whom correspondence should be sent:

Kalliopi A. Roubelakis-Angelakis

Department of Biology, University of Crete, Voutes University campus, 70013 Heraklion, Greece

poproube@biology.uoc.gr

+30-2810-394072

Ky Young Park

Department of Biology, Sunchon National University, 57922, Chonnam, South Korea

plpm@sunchon.ac.kr

+82-61-750-3617

Panagiotis N. Moschou

Department of Plant Biology and Linnean Center of Plant Sciences, Swedish University of Agricultural Sciences, Uppsala BioCentrum, Sweden

panagiotis.moschou@slu.se

+46-700-780553

Author contributions

Conceptualization: KAR-A, PNM; Research desing: KAR-A, KYP, PNM; Research execution: KG, YJK, PNM, EA, CV, AR; Manuscript writing and revision: KAR-A, KG, PNM, KYP.

Funding

This research was funded by EU and the Greek National funds, Research Funding Program THALES (MIS 377281 to K.A.R.-A.), by Korea Research Institute of Bioscience and Biotechnology (to K.Y.P.), by the Swedish Research Council VR and

29 Carl Tryggers Stiftelse för Vetenskaplig Forskning (to P.N.M.), and it was
30 implemented in the frame of COST Actions FA1106 and BM1307.

31

An NADPH-oxidase/Polyamine Oxidase Feedback Loop Controls Oxidative Burst Under Salinity

Katalin Gémes[*1,5], Yu Jung Kim[*2], Ky Young Park[2], Panagiotis N. Moschou[3], Efthimios Andronis[1], Chryssanthi Valassaki[3], Andreas Roussis[3], Kalliopi A. Roubelakis-Angelakis[1]

[1]Department of Biology, University of Crete, Voutes University campus, 70013 Heraklion, Greece (K.G., E. A., K.A.R.-A.)

[2]Department of Biology, Sunchon National University, 57922, Chonnam, South Korea (Y.J.K., K.-Y.P.)

[3]Department of Plant Biology and Linnean Center of Plant Sciences, Swedish University of Agricultural Sciences, Uppsala BioCentrum, Sweden (P.N.M.)

[4]Department of Biology, National & Kapodistrian University of Athens, Panepistimioupolis, Ilissia, Athens, Greece (C.V., A.R.)

[5]Biological Research Centre, Hungarian Academy of Sciences, H-6726 Szeged, Temesvarikrt. 62, Hungary (K.G.)

*Equally contributed

One-sentence Summary:

The tobacco plasma membrane NADPH-oxidase and the extracellular polyamine oxidase interact functionally to regulate homeostasis of reactive oxygen species

Abstract

The apoplastic polyamine oxidase (PAO) catalyzes oxidation of the higher polyamines (PAs), spermidine (Spd) and spermine (Spm), contributing to hydrogen peroxide (H_2O_2) accumulation. However, it is yet unclear whether apoplastic PAO is part of a network which coordinates the accumulation of reactive oxygen species (ROS) under salinity or if it acts independently. Here we unravel that NADPH-oxidase and apoplastic PAO cooperate to control accumulation of H_2O_2 and superoxides ($O_2^{\cdot-}$). To examine to what extent apoplastic PAO constitutes a part of a ROS-generating network, we examined ROS accumulation in guard cells of plants overexpressing or downregulating apoplastic PAO (lines S2.2 and A2, respectively) or downregulating NADPH-oxidase (AS-*NtRbohD*/*F*). The H_2O_2-specific probe BES-H_2O_2 showed that under salinity H_2O_2 increased in S2.2 and decreased in A2 line, compared to wild-type (WT). Surprisingly, the $O_2^{\cdot-}$ specific probe BES-So showed that $O_2^{\cdot-}$ levels correlated positively with that of apoplastic PAO, that is, high/low levels in S2.2 and A2, respectively. By using AS-*NtRbohD/F* lines and a pharmacological approach, we could show that H_2O_2 and $O_2^{\cdot-}$ accumulation at the onset of salinity stress was dependent on NADPH-oxidase, indicating that NADPH-oxidase is upstream of apoplastic PAO. Our results suggest that NADPH-oxidase and the apoplastic PAO form a feedforward ROS amplification loop, which impinges on oxidative state and culminates in the execution of programmed cell death (PCD). We propose that PAO/NADPH-oxidase loop is a central hub in the plethora of responses controlling salt stress tolerance, with potential functions extending beyond stress tolerance.

Introduction

Several enzymatic and non-enzymatic reactions control the production of reactive oxygen species (ROS; Gilroy et al., 2014; Foyer and Noctor, 2016). Superoxide ions ($O_2^{\cdot-}$) are generated mainly by the respiratory burst oxidase homologs NADPH-oxidases (encoded by the *Rboh* genes), and $O_2^{\cdot-}$ dismutation by superoxide dismutase (SOD) is considered as one of the major routes for subsequent hydrogen peroxide (H_2O_2) production (Torres et al., 2002; Kwak et al., 2003; Wang et al., 2013; Baxter et al., 2014).

Homeostasis of ROS is controlled by low molecular weight inter- and intramolecular compounds, such as the polyamines (PAs). PAs are highly reactive aliphatic polycations; main PAs in plants are the diamine putrescine (Put), and the so-called higher PAs, spermidine (Spd; triamine) and spermine (Spm; tetramine; Tiburcio et al., 2014; Saha et al., 2015 and references therein). PAs homeostasis affects a vast range of dynamic developmental and metabolic processes (Paschalidis and Roubelakis-Angelakis, 2005a,b; Wu et al., 2010; Moschou et al., 2009; 2014; Tiburcio et al., 2014; Pal et al., 2015). Oxidation of PAs is catalyzed by amine oxidases (AOs). AOs, such as the diamine oxidases (DAOs or copper containing AOs) and the flavin containing PA oxidases (PAOs), localize either inter- (i.e. apoplast) or intracellularly (i.e. cytoplasm and peroxisomes). DAOs oxidize mainly Put, but also Spd and Spm (with much lower efficiency) yielding H_2O_2 and aminoaldehydes. The apoplastic PAOs terminally oxidize Spd and Spm yielding aminoaldehydes and H_2O_2, while the intracellular ones (referred also as back-converting ones) oxidize PAs to produce H_2O_2, an aminoaldehyde and a PA with one less aminogroup (in the order tetramine->triamine->diamine; Angelini et al., 2010; Pottosin and Shabala, 2014). Through their catabolic oxidative deamination, PAs increase the intra- and extracellular H_2O_2 load.

Under physiological or stress conditions, the rate of ROS generation/scavenging determines their steady level; this rate is integrated into a multitude of vital signaling cues. ROS seem to be multi-faced players; at low levels they are efficiently scavenged by enzymatic and non-enzymatic antioxidants, present in nearly all cellular compartments (Mittler et al., 2004; Miller et al., 2010; Suzuki et al., 2012; Baxter et al., 2014; Foyer and Noctor, 2015); at medium levels and up to a threshold 'signature' ROS participate in downstream signaling cascades that activate

stress protective effector genes/mechanisms; when a certain upper value is reached, oxidative stress is established and ROS participate in a plethora of destructive pathways that culminate in the induction of programmed cell death (PCD) (Moschou et al., 2008a,b; Gémes et al., 2011; Moschou and Roubelakis-Angelakis, 2014).

PAOs and NADPH-oxidases, major ROS generators, have been mostly studied separately and it remains unknown whether they are functionally linked. Their involvement in similar processes points at their possible interplay. Perhaps the best example of convergent action of PAOs and NADPH-oxidases is the control of stomatal aperture. In Arabidopsis guard cells, ABA-induces production of H_2O_2 arising from $O_2^{\cdot-}$ generated by NADPH-oxidases. The produced H_2O_2 activates among others downstream ROS-dependent Ca^{2+} channels contributing to cytosolic Ca^{2+} increase (Kwak et al., 2003; Desikan et al., 2004; Baxter et al., 2014). Likewise, ABA-induces increase of H_2O_2 in the apoplast through the upregulation of peroxidase and apoplastic PAO (Zhu et al., 2006).

In an attempt to increase our understanding of how PAOs can contribute to processes where NADPH-oxidases are involved, we examined the interplay between these genes/enzymes. To this end, we used tobacco plants up-/down regulating apoplastic PAO (lines S2.2 and A2, respectively; Moschou et al., 2008a,b), and tobacco plants downregulating two NADPH-oxidase genes (AS-*NtRbohD* and AS-*NtRbohF*; Ji and Park, 2011). We used guard cells for real-time *in vivo* monitoring of apoplastic PAO/NADPH-oxidase-derived H_2O_2 and $O_2^{\cdot-}$, intra- and intercellularly (Song et al., 2014). Our results provide evidence for an interplay of PAO/NADPH-oxidase that is important for balancing the ratio of intra- and intercellular $O_2^{\cdot-}$ and H_2O_2 levels.

Results

Apoplastic PAO represents the main Spd oxidation source

Considering the large number of AOs in plants (Moschou et al., 2008c), we aimed at determining the relative contribution of apoplastic *versus* intracellular PAs oxidation to H_2O_2 production during salinity. We previously established that during salt stress Spd is secreted into the apoplast where it is oxidized by the apoplastic PAO (Moschou et al., 2008b). However, the contribution of intracellular AOs to Spd oxidation under the same conditions was not examined. In an attempt to dissect the contribution of different AOs to H_2O_2 production, we used tobacco transgenic lines overexpressing or downregulating *ZmPAO* [S-*ZmPAO* (line S2.2) and AS-*ZmPAO* (line A2), respectively; Moschou et al., 2008a,b]. Line S2.2 shows increased while A2 reduced apoplastic PAO activity [results herein and in Moschou et al. (2008b)]. In contrast to our previous works, herein we used leaves that were not fully expanded, in order to take into consideration, the importance of PAOs in developmental processes, such as leaf expansion during salt stress (Rodríguez et al., 2009). At this stage, the profile of PAs in WT, A2 and S2.2 was somewhat different to what has been described previously (**Supplemental Figure 1**; Moschou et al., 2008a,b). However, the observed expected increase of PAs in A2 and the decrease of higher PAs (Spd and Spm) in S2.2 suggest that the apoplastic PAO controls PA levels in expanding leaves, as it was the case for the fully expanded ones (Moschou et al., 2008a,b).

Next, we determined the total cellular capacity of Spd-oxidation (terminal plus back-conversion) *versus* terminal Spd-oxidation in WT, A2 and S2.2. To achieve this, we developed an in-gel Spd-oxidation assay that determines total Spd-oxidation activity. We compared the results obtained from this in-gel Spd-oxidation assay, to those obtained from a colorimetric assay that determines terminal Spd-oxidation (**Supplemental Figure 2A**). The in-gel assay is based on the fact that H_2O_2 produced by Spd-oxidation reacts with 3,3'-diaminobenzidine (DAB), forming a brownish adduct that denotes the gel regions (bands) enriched in Spd-oxidase activity. In WT, Spd-oxidase can be visualized as multiple bands (3 main ones), with a major isoenzyme (>50%) showing high mobility (referred hereafter as anodal). This isoenzyme pattern is consistent with the large number of predicted PAOs and DAOs in tobacco genome (at least 1 apoplastic and 4 intracellular PAOs and >12 DAOs; **Supplemental File 1**). However, we could not define a large number of bands in WT,

suggesting that some isoenzymes may show similar mobility on the gel preventing their separation, may not be present in leaves, or could be refractory to this analytical method. In A2, the major anodal Spd-oxidase isoenzymes were depleted suggesting that they most likely correspond to apoplastic PAO isoforms (**Supplemental Figure 2A,B**). In S2.2, we observed a significant increase of the in-gel Spd-oxidase potential, and in particular the appearance of an additional fast migrating band that could not be seen in WT and A2. Although we could only achieve a fair resolution of isoenzymes, we assume that the fast migrating band corresponds to the apoplastic maize PAO isoenzyme, which is overexpressed in S2.2 (predicted molecular weight ca. 53 kD). We could also observe in S2.2 an increase of additional bands, which were significantly less mobile than the band that presumably corresponds to maize PAO. These isoenzymes could correspond to post-translationally modified maize PAO or different maize PAO fractions (Cona et al., 2006). Alternatively, the increase in apoplastic PAO may signal upregulation of other AOs or simply the DAB adduct, due to its higher production in S2.2, may diffuse producing erroneous bands. Quantification of bands in the three genotypes showed that the overall Spd-oxidase activity in S2.2 increased significantly by 2-fold, mostly due to the increase of the anodal isoenzymes; A2 lines showed a 2-fold decrease due to the absence of the major anodal isoenzyme. Taken together, these results suggest that the apoplastic PAO represents the major Spd-oxidase activity.

In the colorimetric assay, DAO activity (terminal oxidation of Put) was not significantly increased among the three genotypes (**Supplemental Figure 2C**). On the other hand, the terminal Spd-oxidase activity (mainly apoplastic PAO) was significantly reduced in A2 lines, while in S2.2 it increased by 3-fold (**Supplemental Figure 2C**). In addition, apoplastic PAO activity was highly responsive to 200 mM salt treatment (referred hereafter as NaCl treatment) exhibiting significant increase (Moschou et al., 2008b), whereas the cathodal total Spd-oxidase activity responded moderately to NaCl treatment **(Supplemental Figure 2B, C**).

To further substantiate the previous finding, we examined the Spd-oxidase activity of protoplasts by the colorimetric 4-aminopterine oxidation assay used to determine the activity of both terminal and back-converting PAOs and DAOs (Tavladoraki et al., 2006). The activity of Spd-oxidase in WT protoplasts was negligible [close to background levels (as a positive control, purified AtPAO3 was used in these assay; Moschou et al., 2008c)] suggesting that the main Spd-oxidase

activity resides in the apoplastic compartment. Taken together, the data produced through the in-gel and the *in vitro* assays, suggest that the apoplastic PAO accounts for at least 50% of the total Spd-oxidase activity in expanding tobacco leaves, and therefore, it is the major Spd oxidase activity during salinity.

Apoplastic PAO impacts $O_2^{\cdot-}$ production

Previously, we found that S2.2 plants show increased SOD activity suggesting that $O_2^{\cdot-}$ homeostasis may be compromised in these plants (Moschou et al., 2008a). NaCl treatment can be used to examine the contribution of apoplastic PAO to H_2O_2 levels and the *in situ* ROS detection assay is a powerful tool in the estimation of PAO-derived H_2O_2 levels (Moschou et al., 2008a,b). Under control conditions, we could not detect significant differences in the staining intensities for $O_2^{\cdot-}$ and H_2O_2 among the three genotypes (**Figure 1A,B**; 0 h). NaCl treatment induced the increase of both ROS in a time-dependent manner. One to 24 h post-treatment, A2 leaves contained lower, while S2.2 leaves contained higher levels of $O_2^{\cdot-}$ and H_2O_2 than WT (**Figure 1A, B**; 1 h). These results were confirmed by using an *in vitro* quantification assay for H_2O_2 (**Figure 1C**), and suggest that apoplastic PAO influences the production of, not only H_2O_2, but also of $O_2^{\cdot-}$ under stress conditions.

The apoplastic PAO-dependent ROS accumulation is sufficient to induce PCD within the first few hours of NaCl treatment

226 We have shown that apoplastic PAO is critically required for PCD execution during
227 prolonged NaCl stress (stress treatment in the range of several days; Moschou et al.,
228 2008b). Here we examined to what extent under short-term NaCl treatments (in the
229 range of hours) apoplastic PAO-generated ROS are sufficient to induce PCD
230 hallmarks. The array of events that precede PCD execution during NaCl stress are yet

231 unclear and might be context/species specific. S2.2 showed an early accumulation of
232 oxidized proteins (**Supplemental Figure 3A-B**; 1 h post-treatment) in contrast to A2.
233 Significant accumulation of necrotic cells was observed 6 h post-treatment and
234 onwards (**Supplemental Figure 3C**). Thus, accumulation of oxidized proteins and
235 ROS seem to precede PCD. Our results suggest that short NaCl treatments (i.e. <24 h)

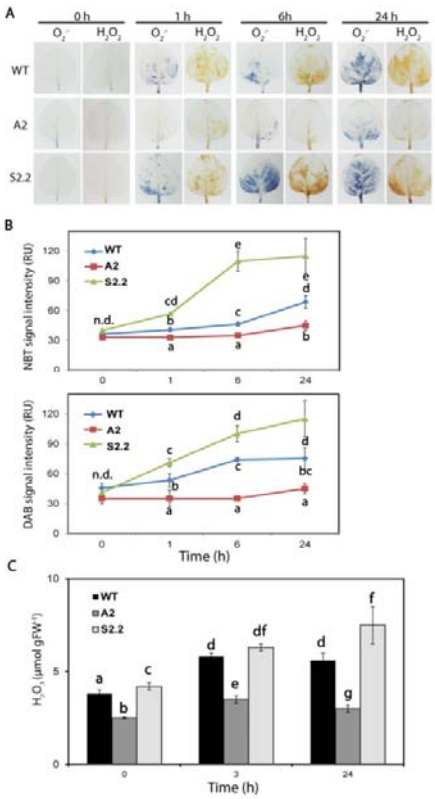

Figure 1. *In situ* ROS detection in the leaves of WT, A2 and S2.2 plants post-NaCl treatment.

(A) *In situ* detection of $O_2^{\cdot-}$ (blue) and H_2O_2 (brown) levels 1, 6 and 24 h post-NaCl treatment. Images are from a single representative experiment replicated three times.

(B) Quantification of blue and brown signal from the *in situ* detection. NBT, nitroblue tetrazolium; DAB, 3,3'-diaminobenzidine. RU, relative units.

(C) H_2O_2 levels in leaves, 3 h and 24 h post-NaCl treatment.

Data in (B) and (C) are means±SE of three biological replicates with three technical replicates each. Different letters indicate significant differences of Duncan's multiple comparisons ($P<0.05$).

are enough to induce apoplastic PAO-derived ROS accumulation of sufficient amount to induce PCD hallmarks. In addition, our results suggest that protein oxidation and accumulation of ROS are upstream events in the execution of NaCl-induced PCD, at least under the described conditions.

Guard cells reflect the real-time ROS accumulation post-NaCl-treatment

Guard cells have been used to study real-time ROS accumulation (Song et al., 2014). In these cells, the NADPH-oxidase genes *RbohD* and *RbohF* are involved in abscisic acid (ABA)-mediated stomatal closure (Zhang et al., 2001; Kwak et al., 2003; Song et al., 2014). Similarly, apoplastic PAO contributes to ABA-induced H_2O_2 production in maize under control conditions (Xue et al., 2008).

Firstly, we used the unspecific ROS probe DCFDA (2',7'-dichlorofluorescein diacetate) to determine ROS production in guard cells. DCFDA is hydrolyzed by cellular esterases to form DCFH, which is oxidized in the presence of peroxidases by hydroxyl or organic peroxyl radicals and the reactive nitrogen species $NO^{\cdot}$ and ONOO– to form the fluorescent dye dichlorofluorescein (DCF; Myhre et al., 2003). The intensity of DCF reflects the formation of general reactive species (RS; sum of nitrogen and oxygen reactive species) rather than specific ones, providing a rough estimate of ROS production. In guard cells of WT, A2 and S2.2 fluorescence of DCF coincided with the total H_2O_2 and $O_2^{\cdot-}$ production determined using the *in situ* detection method (**Figure 2A**). In particular, under control conditions, no significant differences were observed in DCF fluorescence in guard cells among the three genotypes (**Figure 2A-C; 0 h**). Thus, under control conditions apoplastic PAO does not seem to influence the RS levels. However, 1- and 6 h post-treatment, S2.2 contained higher, while A2 lower DCF compared to WT (**Figure 2A-C**; **1 and 6 h**). DCF accumulated mainly in the nucleus and chloroplasts, but also at the cell margins of S2.2 guard cells (**Figure 2C; 6 h**). This accumulation pattern does not necessarily reflect the RS production sites. In accordance, previous studies suggested that different ROS probes tend to accumulate to distinct intracellular sites which may not coincide with the ROS producing sites [e.g. Snyrychova et al., (2009)].

Next, we used more specific dyes to estimate H_2O_2 levels in guard cells. To this end, we evaluated two different sets of fluorescent probes. First, we used the H_2O_2-probes Amplex Red (AR) and Amplex Ultra Red (AUR; Ashtamker et al., 2007), which are used to estimate H_2O_2 levels intra- and extracellularly, respectively. Under control conditions, no significant differences could be observed among the three genotypes in AR and AUR fluorescent intensities (**Supplemental Figure 4A, B; 0 h**). One and 6 h post-treatment with NaCl, an increase in AR and AUR fluorescence was detected in all three genotypes, mostly in S2.2 plants (**Supplemental Figure 4A**). Significant AR and AUR fluorescent signals accumulated in chloroplasts. A2 plants

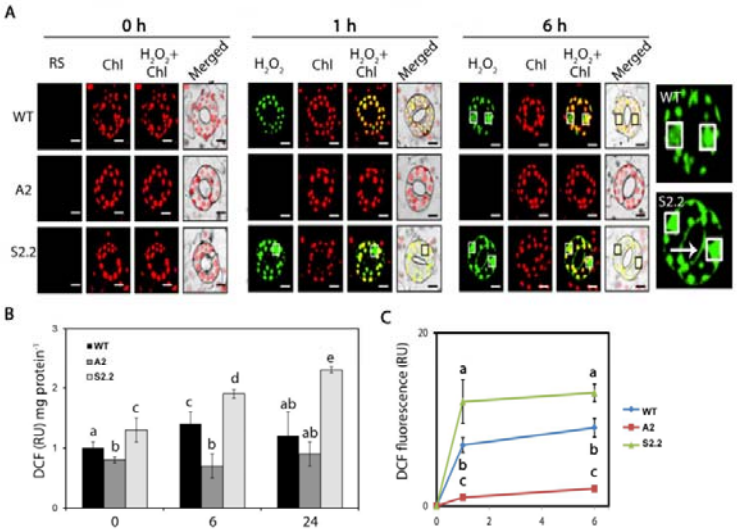

Figure 2. RS detection in guard cells of WT, A2 and S2.2 plants post-NaCl treatment.

(A) Representative CLSM images of DCF fluorescence (green; DCFDA staining) and chlorophyll autofluorescence (red) at 0, 1 and 6 h post-NaCl treatment. White rectangular (black in merged images) denote nuclei. Images on the right, show enlarged versions of WT and S2.2 guard cells (6 h). Arrow indicates the signal accumulation on the cell margins. Images are from a single representative experiment replicated three times. Scale bars, 20 µm.

(B) DCF fluorescence quantification in leaf extracts.

(C) Time course quantification of DCF fluorescence in (A).

Data in (B) and (C) are means±SE of three biological replicates with three technical replicates each. Different letters indicate significant differences of Duncan's multiple comparisons ($P<0.05$). RU, relative units.

showed reduced AR and AUR fluorescence (6 h), preceded by a transient increase of AUR 1 h post-treatment. This transient increase, may reflect the presence of high levels of peroxidase in the apoplast of A2 plants or the interference of the probe with a cellular metabolite. Snyrychova et al. (2009) showed that AR and AUR are highly

sensitive to peroxidase levels, similarly to the DCF and DAB that are also highly sensitive to peroxidase (Noctor et al., 2016).

Next, we employed a peroxidase-independent method for estimation of H_2O_2 levels. We used the highly specific benzene sulfonyl (BES)-H_2O_2 and BES-H_2O_2-Ac probes to estimate intra-/extracellular H_2O_2 levels, respectively (**Figure 3**). This probe pair is converted to fluorescent molecules in the presence of esterases and might be more specific than AR and AUR that are more extensively used in the *in vitro* determinations of H_2O_2 where peroxidases are added in surplus (Noctor et al., 2016). By using BES-H_2O_2 and BES-H_2O_2-Ac we observed a similar trend of H_2O_2 accumulation in S2.2 (**Figure 3A, B**). However, in this case we did not observe the transient increase of H_2O_2 in A2 1 h post-treatment (**compare Figure 3B with Supplemental Figure 4B**). Taken together, our results confirm that guard cells can be efficiently used to monitor real-time ROS accumulation. In addition, guard cells offer some unique advantages over other cell tissue/types for ROS detection. They are homogeneous, readily accessible for microscopic observation, and they show a profound physiological responsiveness to short-term NaCl treatment. In addition, we confirm that BES-H_2O_2 and BES-H_2O_2-Ac are more specific probes for detection of H_2O_2 levels in plants. Nevertheless, a careful assessment of different probes might be required depending on the context/tissue.

PAO-derived H_2O_2 coincides with $O_2^{\cdot-}$ production in guard cells

Intracellular generation of $O_2^{\cdot-}$ was detected using BES-So-AM, a highly specific fluorescent probe for $O_2^{\cdot-}$ (Maeda et al., 2007). Under control conditions, no significant accumulation of O_2.- could be detected in the three genotypes (**Figure 4A; 0 h**). One and 6 h post-treatment, the levels of intracellular $O_2^{\cdot-}$ were significantly increased in guard cells of WT and S2.2 plants, compared to A2 plants (**Figure 4A; 1 h and 6 h**). Particularly, fluorescent BES-So-AM accumulated in the nucleus and chloroplasts of WT. BES-So-AM was also detected in cell margins of S2.2 guard cells. Thus, although 1 h post-NaCl treatment pixel intensity of BES-So-AM fluorescence marginally differed between WT and S2.2, the difference in the total intracellular levels of fluorescent BES-So-AM was very big, as estimated by counting total number of pixels pseudocolored green [in arbitrary units: 50±10 for WT, 10±2 for A2 153±32 for S2.2; see also Materials and Methods]. The previous result is due to additional BES-So-AM in the cell margins of S2.2 plants.

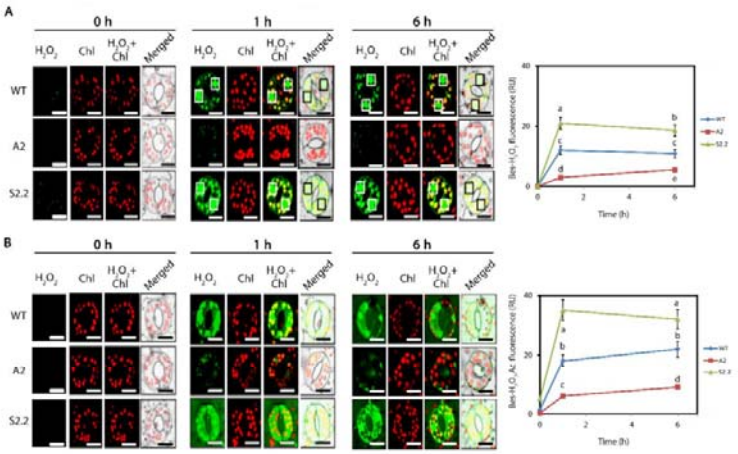

Figure 3. Intra-/extracellular H_2O_2 in guard cells of WT, A2 and S2.2 plants post-NaCl treatment.

(A) Representative CLSM images of intracellular BES-H_2O_2-Ac fluorescence (green) and chlorophyll autofluorescence (red) at 0, 1 and 6 h post-NaCl treatment. White rectangular (black in merged images) denote nuclei. Images are from a single representative experiment replicated three times. Quantification of green signal is shown on the right. Scale bars, 20 µm.

(B) Representative CLSM images of intercellular BES-H_2O_2 fluorescence (green) and chlorophyll autofluorescence (red) at 0, 1 and 6 h post-NaCl treatment. White rectangular (black in merged images) denote nuclei. Images are from a single representative experiment replicated three times. Quantification of green signal is shown on the right. Scale bars, 20 µm.

Data in charts are means±SE of three biological replicates with three technical replicates each. Different letters indicate significant differences of Duncan's multiple comparisons ($P<0.05$). RU, relative units.

3

Next, we used BES-So to detect extracellular $O_2^{\cdot-}$. Similarly to the intracellular $O_2^{\cdot-}$, no significant accumulation of BES-So could be detected under control conditions in the three genotypes (**Figure 4B**; **0 h**). One h post-treatment, the extracellular BES-So fluorescence significantly increased in S2.2 and WT, while it increased moderately in A2 (**Figure 4B; 1 h**). Six h post-treatment, BES-So

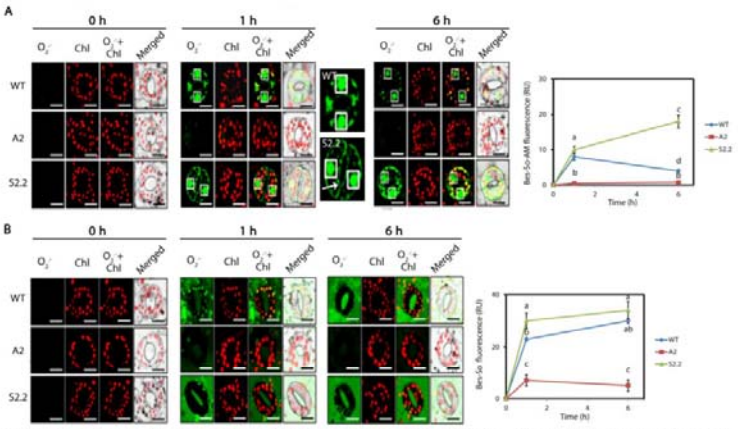

Figure 4. Intra-/extracellular $O_2^{\cdot-}$ in guard cells of WT, A2 and S2.2 plants post-NaCl treatment.

(A) Representative CLSM images of intracellular BES-So-Am fluorescence (green) and chlorophyll autofluorescence (red) at 0, 1 and 6 h post-NaCl treatment. White rectangular (black in merged images) denote nuclei. Images next to 1 h time-point panel, show enlarged versions of WT and S2.2 guard cells. Arrow indicates the signal accumulation on the cell margins. Images are from a single representative experiment replicated three times. Quantification of green signal is shown on the right. Scale bars, 20 µm.

(B) Representative CLSM images of intercellular BES-So fluorescence (green) and chlorophyll autofluorescence (red) at 0, 1 and 6 h post-NaCl treatment. White rectangular (black in merged images) denote nuclei. Images are from a single representative experiment replicated three times. Quantification of green signal is shown on the right. Scale bars, 20 µm.

Data in charts are means±SE of three biological replicates with three technical replicates each. Different letters indicate significant differences of Duncan's multiple comparisons ($P<0.05$). RU, relative units.

fluorescence increased further in WT and mainly in S2.2, but not in A2 (**Figure 4B; 6h**). Our results indicate that apoplastic PAO levels positively correlate with $O_2^{\cdot-}$ levels in guard cells.

Apoplastic PAO levels correlate with NADPH-oxidase activity

The correlation between PAO and $O_2^{\cdot-}$ levels in our experiments, prompted us to examine the genetic interaction between *PAO* and two of the major NADPH-oxidase genes in guard cells, *RbohD* and *RbohF* (Song et al., 2014). Under control conditions, mRNA levels of *RbohD*/*F* were significantly increased in S2.2 compared to WT, but not in A2 (**Figure 5A**). One and 6 h post-NaCl treatment, the mRNA levels of *RbohD* tended to increase in all genotypes (**Figure 5A; 1 and 6 h**). The same trend, although to a lesser extent, was observed in all genotypes for mRNA levels of *RbohF*. However, 6 h post-NaCl treatment, the mRNA levels of *RbohF* slightly decreased in all genotypes compared to 1 h. Under both control and NaCl-treatment, the higher mRNA levels of *RbohD*/*F* in S2.2 were accompanied by increased in-gel activity of NADPH-oxidase, while A2 showed a marked decrease (**Figure 5B, C; 1 h**).

PAO-mediated ROS production depends on NADPH-oxidase

Further, we examined the physiological effect of *RbohD/F* downregulation in ROS production using plants with silenced *RbohD* or *RbohF* (AS-*NtRbohD* and AS-*NtRbohF*; Ji and Park, 2011). We observed that *RbohF* and *RbohD* mRNA were also reduced in AS-*NtRbohD* and AS-*NtRbohF* (**Supplemental Figure 5**), respectively. The mRNA of *RbohD* and *RbohF* share high sequence similarity (81%; query coverage 89%), suggesting that the antisense cDNA of *RbohD* and *RbohF*, can downregulate *RbohF* and *RbohD*, respectively. Therefore, we refer to these transgenics hereafter as AS-*NtRbohD/F*. Importantly, under control and post-NaCl treatment conditions, the AS-*NtRbohD/F* plants showed similar to WT apoplastic *NtPAO* (**Supplemental Figure 5**). Interestingly, neither $O_2^{\cdot-}$ as expected, but more importantly nor H_2O_2 significantly accumulated post-NaCl treatment in the two transgenic genotypes under control and stress conditions (**Figure 6** and **Figure 7**). These results point to the importance of NADPH-oxidase in the production of ROS under short-term NaCl treatment.

In order to confirm the previous result and examine the contribution of PAO/NADPH-oxidase to a presumamble sustained H_2O_2 accumulation, we used a pharmacological approach. We used the potent inhibitors diphenyleneiodonium (DPI; 50 μm) and guazatine (Guaz; 5 μm), to inhibit NADPH-oxidase and PAO, respectively. Our guard cell assay cannot be used to assay sustained H_2O_2 accumulation, since even the untreated leaf strips die out after approximately 12 h. In order to estimate H_2O_2 for a prolonged time (up to 72 h), we used whole leaves. In all

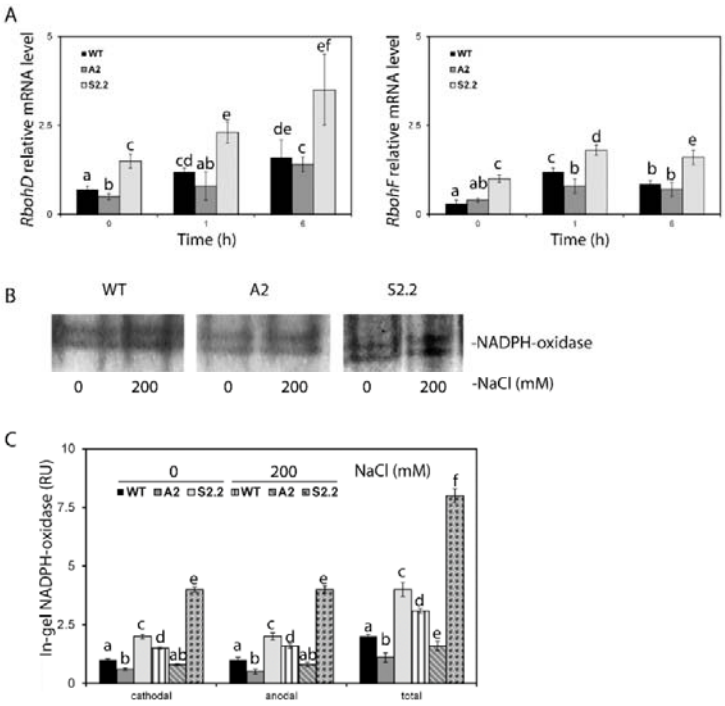

Figure 5. mRNA levels and activity of NADPH-oxidase in WT, A2 and S2.2 plant leaves post-NaCl treatment.

(A) Abundance of mRNA levels of *RbohD* (left) and *RbohF* (right) in leaves post-NaCl treatment with 200 mM NaCl.

(B) Representative gel images showing the in-gel activity assay of NADPH-oxidase 1 h post-NaCl treatment with 200 mM NaCl. Images are from a single representative experiment replicated three times.

(C) Quantification of anodal and cathodal isoenzymes of NADPH-oxidase. Similar isoenzyme pattern has been previously reported in *N. tabacum* (Sagi and Fluhr, 2001). Data in (A) and (C) are means±SE of three biological replicates. Different letters indicate significant differences of Duncan's multiple comparisons ($P<0.05$). RU, relative units.

genotypes, DPI ameliorated NaCl-induced H_2O_2 production (**Supplemental Figure 6**). These data point that NADPH-oxidase contributes significantly to the accumulaton of H_2O_2. In the presence of Guaz and NaCl, H_2O_2 accumulation was induced relative to control, albeit to a lesser extent. The strong effect of DPI at early time points (compare 6 h with 72 h) indicates the importance of NADPH-oxidase for ROS

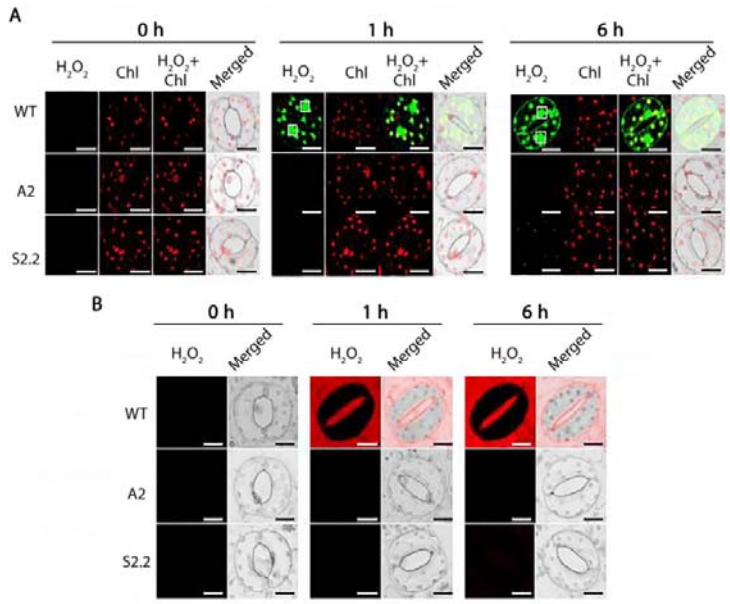

Figure 6. Intra-/extracellular H_2O_2 in guard cells of WT, AS-*NtRbohD* and AS-*NtRbohF* plants post-NaCl treatment.

(A) Representative CLSM images of intracellular BES-H_2O_2-Ac fluorescence (green) and chlorophyll autofluorescence (red) at 0, 1 and 6 h post-NaCl treatment. White rectangular denote nuclei. Images are from a single representative experiment replicated three times. Scale bars, 20 μm.

(B) Representative CLSM images of intercellular AUR fluorescence (red) at 0, 1 and 6 h post-NaCl treatment. Scale bars, 20 μm.

homeostasis at the onset of stress. As expected, the accumulation of H_2O_2 was further inhibited by the simultaneous addition of both DPI and Guaz, supporting the notion that the two enzymes cooperate constituing a feedforward ROS amplification loop.

We should note that DPI inhibits PAO activity among others; however, the potency of this inhibition is much weaker than that of Guaz (Moschou et al., 2008c).

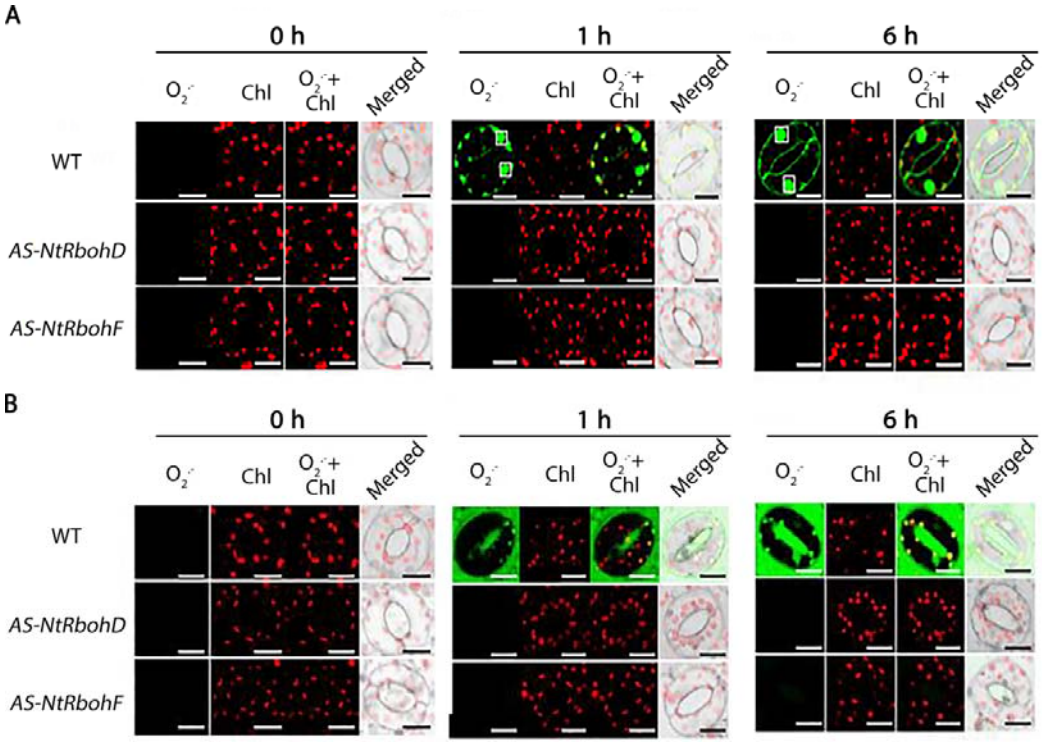

We estimated the activity of PAO in the presence of DPI or Guaz. Under our experimental conditions, in WT and S2.2, DPI inhibited slightly the apoplastic PAO activity (ca. 15%; **Supplemental Figure 7**). However, Guaz nullified the activity of PAO in both genotypes within 6 h. We assume that the weak inhibitory effect of DPI on PAO is not significant.

Discussion

In this work, we studied the contribution of the apoplastic PAO and the plasma membrane NADPH-oxidase to ROS accumulation and how their cross-talk regulates ROS homeostasis. Building on the unexpected observation that PAO regulates $O_2^{\cdot-}$ accumulation, results presented herein allow to propose a model in which a feedforward amplification loop that involves apoplastic PAO and NADPH-oxidase controls ROS accumulation. Our model integrates the observations that apoplastic PAO positively influences the activity of NADPH-oxidase and that NADPH-oxidase is upstream of PAO in the relay of events that control ROS accumulation. By detailing the relationship between PAO and NADPH-oxidase, we could show the absolute requirement of NADPH-oxidase for ROS production within the first few hours of NaCl treatment. The apoplastic PAO functions as an amplifier of the initial NADPH-oxidase ROS accumulation. Taken together, our model suggests that the apoplastic PAO feeds a stress-inducible ROS amplification loop that can lead to ROS accumulation above a toxicity threshold, culminating to PCD. Our findings allow to extend our understanding of how apoplastic PAOs control tolerance responses during stresses. Notably, the tissue-wide role of NADPH-oxidase and apoplastic PAO in ROS regulation can be detailed in a single-cell context, the guard cells, by the careful selection of specific ROS probes. The observed positive correlation between $O_2^{\cdot-}$ and apoplastic PAO levels upon short-term NaCl treatment at an organ level (leaf; **Figure 1**), could be extrapolated in guard cells (**Figures 2-4**). This finding simplifies analyses of ROS accumulation, considering the unique advantages of guard cells as a study system: accessibity for microscopical studies and homogenicity. The latter reason can be quite important considering that different cell types can have different contributions to ROS levels.

But to what extent are the NADPH-oxidase and apoplastic PAO important for guard cell physiology? It has been well established that both of them contribute to the regulation of stomatal aperture and this role is executed through their intristic relation to ROS (Zhang et al., 2009; Fincato et al., 2012 and references therein). Loss of RBOHF in Arabidopsis leads to the partial impairment of ABA-induced stomatal closure, which is further reduced and ROS production is abolished in an *AtRbohD/F* mutant, suggesting that the two genes act redudantly in the control of stomatal aperture (Chater et al., 2015). In addition, AOs positively contribute to stomatal closure in grapevine (Paschalidis et al., 2010). In contrast, acetylation of 1,3-

diaminopropane, a product of apoplastic PAO by N-ACETYLTRANSFERASE ACTIVITY1 (NATA1) in Arabidopsis, can result in the slowing of stomatal closure (Jammes et al., 2014). Thus, both enzymes are of critical importance to the physiology of stomatal aperture and may act redundantly or cooperatively in the same ROS network.

Feedforward loops offer an evolutionary conserved solution to the problem of signal amplification (Cordero and Hogeweg, 2006). Their over abundance in signaling networks most likely reflects their incremental acquisition of adaptive single interactions between different components within the network. Plants have evolved a wide array of feedback loops to control a variety of physiological responses upon various exogenous or endogenous signals. For example, salicylate (SA) operates in a feedforward ROS loop that culminates in cell death (Yun and Chen, 2006). Feedforward loops for ROS amplification have been described in non-plants as well, between NADPH-oxidase and mitochondria derived ROS (Graham et al., 2012). These loops are subordinate to additional signals, such as metabolic perturbations (e.g. glucose deprivation). Likewise, the PAO/NADPH-oxidase loop is subordinate to exogenous stress; activation of this loop requires NaCl treatment. In the absence of NaCl, the loop could not be initiated, even though in S2.2 NADPH-oxidase was increased in the controls (**Figure 5**). Indeed, under control conditions, cellular content of $O_2^{\cdot -}$ and H_2O_2 does not differ significantly among WT, A2 and S2.2, as well among WT, AS-*NtRbohD*/*F* (**Figures 1-4**). On the contrary, NaCl treatment increases dramatically both, H_2O_2 and $O_2^{\cdot -}$ in S2.2; these ROS increase moderately in WT and at very low levels in A2, both intra- and extracellularly. Taken together, these suggest that PAO/NADPH-oxidase loop is subordinate to yet unidentified signals.

What is the nature of the signals that bring about the activation of the PAO/NADPH-oxidase loop? Considering that this loop is activated early after the onset of salinity, it is highly unlikely that it is activated by time consuming pathways, such as lengthy transcriptional cascade(s). In fact, accumulating evidence supports that NADPH-oxidase is amenable to several regulatory post-translational modifications (Li et al., 2014). Likewise, apoplastic PAO activity may also be controlled by post-translational modifications. In maize, apoplastic PAO activity is controlled by its phosphorylation status (Cona et al., 2006). An alternative scenario would be that the loop is not induced at all, but its effect is masked by the ROS scavenging machinery. In accordance, an adaptive regulation of the ROS scavenging

machinery has been suggested, to dispose-off surplus H_2O_2 produced by apoplastic PAO during development (Moschou et al., 2008a). This is supported by the absence of significant ROS accumulation in S2.2, although NADPH-oxidase is pre-induced in this line (**Figure 5**). During stress, a transient decrease of the antioxidant machinery may lead to the unmasking of the effect of the PAO/NADPH-oxidase loop that is further enhanced by additional signaling pathways. These two scenarios are not mutually exclusive, and may both be plausible perhaps at different times/phases.

Taking into consideration the potency of the PAO/NADPH-oxidase loop to the overall ROS contribution, the next question is to what extent these ROS signal downstream events. A dedicated set of sensor proteins is involved in the perception of ROS signals (Bosch et al., 2014). These proteins are clustered in networks that mediate signaling events leading to downstream responses, including changes in gene expression and activation of cell death programs. Our work highlights that the PAO/NADPH-oxidase loop has the potential to trigger cell death. Indeed, this loop produces ROS of sufficient quantity to drive protein oxidation and to reach a level of cellular toxicity (**Supplemental Figure 3**). Protein oxidation might be the tip of the iceberg in a myriad of additional cell-wide consequences brought about by PAO/NADPH-oxidase loop, which sets in motion by NaCl treatment and may affect many downstream processes that culminate to cell death execution. Certainly, this loop might just be a hub in a plethora of additional pathways that refine the decision towards cell death. However, it seems likely that the PAO/NADPH-oxidase loop possesses a central regulatory role in the execution of cell death, taking into consideration the tight association between apoplastic PAO levels and cell death levels.

An interesting twist to our story is the possible temporal dependence for a PAO/NADPH-oxidase loop. Application of DPI affected significantly H_2O_2 levels mostly at early time points (6 h), while Guaz had a minor effect that was escalated with time (>24 h; **Supplemental Figure 6**). We speculate that this timely-resolved effect of the two inhibitors may indicate the initial importance of the PAO/NADPH-oxidase loop; then, PAO is uncoupled from NADPH-oxidase and is required for sustaining ROS levels. In support of this, AS-*NtRbohD/F* failed to accumulate $O_2^{\cdot-}$ and H_2O_2 (**Figures 6 and 7**) during the early stages of salinity, although they contained WT-like levels of apoplastic PAO. This finding suggests that NADPH-oxidase is upstream of the apoplastic PAO in ROS regulation and an initial ROS

accumulation by NADPH-oxidase might be important for triggering the activation of the apoplastic PAO pathway. However, we should note that the interaction between PAO/NADPH-oxidases and their feedforward relationships, do not allow at this stage to efficiently disentangle their distinct contribution to ROS levels. Considering that inhibitors may be imposed to differential uptake during different stages of stress, our model regarding the temporal emergence of the loop requires further refinement.

Overall, our data suggest that NADPH-oxidase and the apoplastic PAO are not parallel pathways for ROS production. Instead, they form a nexus and cross-talk in the frame of the strategy of plant cells to regulate ROS homeostasis. In addition, NADPH-oxidase and apoplastic PAO show a feedforward relationship that is, high PAO levels correlate with high NADPH-oxidase activity. Therefore, the two proteins are part of the same ROS homeostatic regulatory module, which affects the extra- and intracellular cross-talk of ROS regulatory mechanisms. However, it is still unclear to what extent intracellular PAOs affect this module. We previously established that in Arabidopsis a peroxisomal PAO cross-talks with NADPH-oxidase to activate the mitochondrial alternative oxidase pathway (AOX; Andronis et al., 2014). To advance our understanding on PAO/NADPH-oxidase cross-talk, the next critical step could be to explore how ROS signals are transduced/perceived for the fine orchestration of this cross-talk and what is the relationship between apoplastic and intracellular PAOs in this regulation.

Materials and Methods

Preparation of transgenic plants and growth conditions

The preparation of transgenic tobacco (*Nicotiana tabacum* cv Xanthi) plants with altered expression of the *Zea mays POLYAMINEOXIDASE* (*ZmPAO*) gene (lines A2*,* S2.2) has been previously described (Moschou et al., 2008a; 2008b). The preparation of transgenic tobacco specifically downregulating the two genes coding NADPH-oxidase, *RbohD* and *RbohF*, was described by Ji and Park (2011). Surface-sterilized transgenic seeds (T3 homozygous) were cultured on solid Murashige and Skoog medium (pH 5.8) and then transferred to soil under light (16/8h photoperiod, 100 μmol photons m^{-2} s^{-1}) at 25 ± 5°C. Two to 3-week old-plants were used.

RNA extraction qPCR

Total RNA preparation was performed as previously described (Wi and Park, 2002). The primers used (Bionics, Korea) are shown in Table S1. One µg of total RNA from leaves was reverse-transcribed for 30 min at 42℃ in a 20 µl reaction volume using a High Fidelity PrimeScript^{TM} RT-PCR kit (Takara, Japan) according to the manufacturer's instructions. The qPCR reactions were carried in Chromo 4^{TM} Continuous Fluorescence Detector (Bio-Rad, USA). Ct values were analyzed using MJ Opticon Monitor Software version 3.1 (Bio-Rad, USA) and then exported to Microsoft Excel for further analysis. The reference gene *β-ACTIN* was used.

Protein extraction, Western blotting, in-gel enzymatic assays and electrophoresis

Proteins were extracted and treated as described in Papadakis and Roubelakis-Angelakis (2005). For NADPH oxidase activity staining, the procedure was carried out according to Carter et al. (2007). An aliquot containing 100 µg of protein from each tissue homogenate was electrophoresed on a 10% native PAGE. The gel was then incubated in 0.5 mg mL^{-1} nitroblue tetrazolium (NBT) in 10 mM Tris, pH 7.4 supplied with 134 mM NADPH until bands were detected. For PAO activity staining, 50 µg of protein extracts were electrophoretically resolved in a 10% polyacrylamide gel. Subsequently, the gel was incubated in 50 mM phosphate buffer (pH 7.0) for 30 min, to which 10 mM Spd was added for a further 10 min. The gel was rinsed and then incubated in 50mM phosphate buffer (pH 7.0) containing 1 mg mL^{-1} 3,3'-diaminobenzidine (DAB). Protein samples that were incubated with 1 uM guazatine prior to electrophoresis were used as negative controls.

PAO and DAO enzymatic assay

The spectrophotometric method developed by Federico et al. (1985) was used for determining apoplastic PAO and DAO activities. Absorbance was read at 460 nm.

Determination of endogenous PAs

PAs were analyzed as described by Goren et al. (1982). Leaves (0.2 g) were homogenized in 0.5 ml of 5% (v/v) perchloric acid (PCA) and centrifuged at 15,000 rpm for 20 min. Then 0.2 mL of saturated sodium carbonate and 0.4 ml of dimethylaminonaphthalene-1-sulfonyl chloride (1 mg mL^{-1} in acetone) were added to 0.2 ml of the supernatant, and the mixture was incubated at room temperature for 24 h in the dark. The dansylated products were extracted with benzene and separated on

thin layer chromatography in chloroform: triethylamine (25:2, v/v). The separated PAs were scraped off and quantified using a spectrophotofluorimeter (RF-1501, Shimadzu, http://www.shimadzu.com), by which the emission at 495 nm was recorded after excitation at 350 nm. Alternatively, PAs were determined as described previously (Kotzabasis et al., 1993) using an HP 1100 high-performance liquid chromatograph (Hewlett-Packard).

Photometric determination of H_2O_2 levels

The endogenous levels of H_2O_2 content of the tissues were determined as described by Sahebani et al. (2009). Fresh leaf material (100 mg) was homogenized in an ice bath with 0.375 mL 0.1% (w/v) trichloroacetic acid (TCA). The homogenate was centrifuged at 7,000 rpm for 20 min and 0.25 mL of the supernatant was added to 0.25 mL 10 mM potassium phosphate buffer (pH 7.0) and 0.5 mL 1 M KI. The absorbance of the supernatant was read at 390 nm. The content of H_2O_2 was determined using a standard curve.

***In situ* detection of ROS**

In situ accumulation of H_2O_2 was detected using the method of Thordal-Christensen et al. (1997) and $O_2^{\cdot-}$ according to Jabs et al. (1996). In addition, NaCl-treated tobacco leaves were incubated for 2 h in NBT staining solution (1 mg mL^{-1}, pH 7.8, 10 mM potassium phosphate buffer) at room temperature. To detect *in situ* accumulation of H_2O_2, NaCl-treated tobacco leaves were incubated for 2h in DAB staining solution (1 mg mL^{-1}, pH 3.8) at room temperature. Tobacco leaves were destained boiling in 96 % (v/v) ethanol and then photographed using a digital camera.

Confocal microscopy detection of ROS in guard cells

For fluorescent detection of ROS, leaf epidermal strips were used. For DCFDA (Sigma Chemicals, St Louis, MO, USA) strips were floated on a solution of 10 mM in 20 mM potassium phosphate buffer (pH 6.0) for 10 min (excitation: 450 ± 490 nm, barrier: 520 ± 560 nm). Amplex red and Amplex ultra red (Invitrogen, USA) were used at a concentration of 50 mM in 50 mM sodium phosphate buffer (pH 6.0) for 1 h in the dark (AR: excitation 571 nm; emission 585 nm, AUR: excitation 568 nm; emission 581 nm). BES-H_2O_2–Ac and BES-H_2O_2 (WAKO Chemicals, USA) were used at a concentration of 50 mM in 20 mM potassium phosphate buffer (pH 6.0) for

1 h in the dark (excitation 485 nm; emission 530 nm). BES-So-Am and BES-So (WAKO Chemicals, USA) were used at a concentration of 20 mM potassium phosphate buffer (pH 6.0) for 1 h in the dark (excitation 505 nm; emission, 544 nm). Fluorescence was observed using the confocal laser scanning microscope FluoView^{TM} 300 (FV 300, OLYMPUS, Japan).

Quantification of DCF in plant extracts

Plant leaves were homogenized with 10 mM Tris buffer (pH 7.2) and then centrifuged at 2,000g for 5 min. The supernatant was incubated with DCFDA at room temperature for 10 min in the dark. DCF fluorescence was detected by a spectrofluorophotometer (excitation 485 nm; emission 525 nm; RF-1501; Shimadzu). Data were expressed as relative fluorescence per mg of protein.

Detection of carbonylated proteins

Total proteins from tobacco leaves were extracted from frozen samples by grounding the tissue to a fine powder and resuspended in protein extraction buffer [50 mM Tris-HCl (pH 7.5), 150 mM NaCl, 1 mM EDTA, 1 mM phenylmethylsulfonyl fluoride (PMSF), protease inhibitors cocktail (Sigma Chemicals, USA)]. The OxyBlot procedure (Millipore, Billerica, MA) was used to perform immunoblot detection of oxidatively modified proteins by the generation of carbonyl groups. Carbonylated proteins were detected and analyzed following derivatization of protein carbonyl groups with 2,4-dinitrophenylhydrazine (DNP). Total proteins from tobacco leaves post-NaCl treatment (10 μg) were separated by SDS-PAGE. Following transfer to a nitrocellulose membrane, DNP-derivatized proteins were detected by an anti-DNP antibody. Oxidation index was calculated by the ratio between total proteins and standard protein of pixel-based integrated densitometric values using the Oxyblot.

Trypan Blue staining

To monitor cell death, NaCl-treated tobacco leaf discs were immersed for 1 min in a boiling solution of 10 mL of lactic acid, 10 mL of glycerol, 10 g of phenol, and 0.4 % (w/v) trypan blue. After leaf discs had cooled down to room temperature, the solution was replaced with 70 % (w/v) chloral hydrate. Leaf discs were destained overnight and then photographed using a digital camera.

610 **Statistical and image analysis**

611 Statistical analysis was carried out with SIGMAPLOT12.0 statistical software. After
612 ANOVA, Duncan's multiple comparisons were performed. Image analysis was done
613 using FIJI software (Schindelin et al., 2012). For image quantifications of NBT and
614 DAB, we selected 10 regions of interest (ROI; five in each leaf side) of the same area
615 (rectangular) and quantified the integrated density in inverted color images. These 10
616 measurements corresponded to a technical replicate. For quantification of fluorescent
617 signals, the same approach was used. For the total green pixel count, we used the
618 Adjust>Color Threshold in FIJI, and regions of interested (ROI) that included the
619 guard cells. For FIJI analyses, methods described in Moschou et al., (2013 and 2016)
620 were used.

621

622 **Supplemental Material**

623 Supplemental Figure 1. Endogenous polyamine levels in the leaves of WT, A2 and
624 S2.2 transgenic plants under control and 24h post-NaCl treatment.

625 Supplemental Figure 2. Polyamine catalytic genes/enzymes in WT, A2 and S2.2
626 transgenic plants under control and post-NaCl treatment.

627 Supplemental Figure 3. PCD hallmarks in WT, A2 and S2.2 leaves post-NaCl
628 treatment.

629 Supplemental Figure 4. Intra-/extracellular H_2O_2 in guard cells of WT, A2 and S2.2
630 plants post-NaCl treatment.

631 Supplemental Figure 5. Relative mRNA levels of *PAO*, *RbohD*, and *RbohF* genes in
632 *AS-NtRbohD* and *AS-NtRbohF* plants post-NaCl treatment.

633 Supplemental Figure 6. H_2O_2 levels in the leaves 6, 24, 48 and 72 h post-NaCl
634 treatment in the absence or presence of DPI, Guaz or both.

635 Supplemental Figure 7. Apoplastic PAO activity in the presence of DPI post-NaCl
636 treatment.

637 Supplemental File 1

638

639 **Acknowledgements**

640 The authors thank Dr Imene Toumi for her assistance in the lab of K.A.R.-A.

641

642 **Figure Legends**

Figure 1. *In situ* ROS detection in the leaves of WT, A2 and S2.2 plants post-NaCl treatment.

(A) *In situ* detection of $O_2^{-}\cdot$(blue) and H_2O_2 (brown) levels 1, 6 and 24 h post-NaCl treatment. Images are representative from three independent experiments with 6 leaf images per genotype in each timepoint.

(B) Quantification of $O_2^{-}\cdot$(blue) and H_2O_2 (brown) signal from the *in situ* detection. NBT, nitroblue tetrazolium; DAB, 3,3'-diaminobenzidine. RU, relative units.

(C) H_2O_2 levels in leaves, 3 h and 24 h post-NaCl treatment.

Data in (B) and (C) are means±SE of three independent experiments with three technical replicates each. Different letters indicate significant differences of Duncan's multiple comparisons ($P<0.05$).

Figure 2. RS detection in guard cells of WT, A2 and S2.2 plants post-NaCl treatment.

(A) CLSM images of DCF fluorescence (green; DCFDA staining) and chlorophyll autofluorescence (red) at 0, 1 and 6 h post-NaCl treatment. White rectangular (black in merged images) denote nuclei. Images on the right, show enlarged versions of WT and S2.2 guard cells (6 h). Arrow indicates the signal accumulation on the cell margins. Images are representative from three independent experiments with 6 micrographs per genotype in each timepoint. Scale bars, 20 μm.

(B) DCF fluorescence quantification in leaf extracts.

(C) Time course quantification of DCF fluorescence in (A).

Data in (B) and (C) are means±SE of three independent experiments with three technical replicates each. Different letters indicate significant differences of Duncan's multiple comparisons ($P<0.05$). RU, relative units.

Figure 3. Intra-/extracellular H_2O_2 in guard cells of WT, A2 and S2.2 plants post-NaCl treatment.

(A) Representative CLSM images of intracellular BES-H_2O_2-Ac fluorescence (green) and chlorophyll autofluorescence (red) at 0, 1 and 6 h post-NaCl treatment. White rectangular (black in merged images) denote nuclei. Images are representative from three independent experiments with 6 micrographs per genotype in each timepoint. Quantification of green signal is shown on the right. Scale bars, 20 μm.

675 (B) CLSM images of intercellular BES-H_2O_2 fluorescence (green) and chlorophyll
676 autofluorescence (red) at 0, 1 and 6 h post-NaCl treatment. White rectangular (black
677 in merged images) denote nuclei. Images are representative from three independent
678 experiments with 6 micrographs per genotype in each timepoint. Quantification of
679 green signal is shown on the right. Scale bars, 20 μm.
680 Data in charts are means±SE of three independent experiments with three technical
681 replicates each. Different letters indicate significant differences of Duncan's multiple
682 comparisons ($P<0.05$). RU, relative units.
683
684 **Figure 4. Intra-/extracellular $O_2^{\cdot-}$ in guard cells of WT, A2 and S2.2 plants post-**
685 **NaCl treatment.**
686 (A) CLSM images of intracellular BES-So-Am fluorescence (green) and chlorophyll
687 autofluorescence (red) at 0, 1 and 6 h post-NaCl treatment. White rectangular (black
688 in merged images) denote nuclei. Images next to 1 h time-point panel, show enlarged
689 versions of WT and S2.2 guard cells. Arrow indicates the signal accumulation on the
690 cell margins. Images are representative from three independent experiments with 6
691 micrographs per genotype in each timepoint. Quantification of green signal is shown
692 on the right. Scale bars, 20 μm.
693 (B) CLSM images of intercellular BES-So fluorescence (green) and chlorophyll
694 autofluorescence (red) at 0, 1 and 6 h post-NaCl treatment. White rectangular (black
695 in merged images) denote nuclei. Images are representative from three independent
696 experiments with 6 micrographs per genotype in each timepoint. Quantification of
697 green signal is shown on the right. Scale bars, 20 μm.
698 Data in charts are means±SE of three independent experiments with three technical
699 replicates each. Different letters indicate significant differences of Duncan's multiple
700 comparisons ($P<0.05$). RU, relative units.
701
702 **Figure 5. mRNA levels and activity of NADPH-oxidase in WT, A2 and S2.2 plant**
703 **leaves post-NaCl treatment.**
704 (A) Abundance of mRNA levels of *RbohD* (left) and *RbohF* (right) in leaves post-
705 NaCl treatment with 200 mM NaCl.
706 (B) Gel images showing the in-gel activity assay of NADPH-oxidase 1 h post-NaCl
707 treatment with 200 mM NaCl. Images are representative from three independent
708 experiments with one technical replicate in each (1 gel).

(C) Quantification of anodal and cathodal isoenzymes of NADPH-oxidase. Similar isoenzyme pattern has been previously reported in *N. tabacum* (Sagi and Fluhr, 2001). Data in (A) and (C) are means±SE of three indepedent experiments with three technical replicates. Different letters indicate significant differences of Duncan's multiple comparisons relative to WT ($P<0.05$). RU, relative units.

Figure 6. Intra-/extracellular H_2O_2 in guard cells of WT, AS-*NtRbohD* and AS-*NtRbohF* plants post-NaCl treatment.

(A) CLSM images of intracellular BES-H_2O_2-Ac fluorescence (green) and chlorophyll autofluorescence (red) at 0, 1 and 6 h post-NaCl treatment. White rectangular denote nuclei. Images are representative of three independent experiments with 6 micrographs per genotype in each timepoint. Scale bars, 20 μm.

(B) CLSM images of intercellular AUR fluorescence (red) at 0, 1 and 6 h post-NaCl treatment. Images are representative of three independent experiments with 6 micrographs per genotype in each timepoint. Scale bars, 20 μm.

Figure 7. Intra-/extracellular $O_2^{\cdot-}$ in guard cells of WT, AS-*NtRbohD* and AS-*NtRbohF* plants post-NaCl treatment.

(A) CLSM images of intracellular BES-So-Am fluorescence (green) and chlorophyll autofluorescence (red) at 0, 1 and 6 h post-NaCl treatment. White rectangular (black in merged images) denote nuclei. Images are representative of three independent experiments with 6 micrographs per genotype in each timepoint. Quantification of green signal is shown on the right. Scale bars, 20 μm.

(B) CLSM images of intercellular BES-So fluorescence (green) and chlorophyll autofluorescence (red) at 0, 1 and 6 h post-NaCl treatment. White rectangular denote nuclei. Images are representative from three independent experiments with 6 micrographs per genotype in each timepoint.

Parsed Citations

Andronis EA, Moschou PN, Toumi, I, and Roubelakis-Angelakis KA (2014) Peroxisomal polyamine oxidase and NADPH-oxidase cross-talk for ROS homeostasis which affects respiration rate in Arabidopsis thaliana. Front Plant Sci 5: 132

Pubmed: Author and Title
CrossRef: Author and Title
Google Scholar: Author Only Title Only Author and Title

Angelini R, Cona A, Federico R, Fincato P, Tavladoraki P, Tisi A (2010) Plant amine oxidases "on the move": an update. Plant Physiol Biochem 48: 560-564

Ashtamker C, Kiss V, Sagi M, Davydov O, Fluhr R (2007) Diverse subcellular locations of Cryptogein-induced Reactive Oxygen Species production in tobacco Bright Yellow-2 cells. Plant Physiol 143: 1817-1826

Pubmed: Author and Title
CrossRef: Author and Title
Google Scholar: Author Only Title Only Author and Title

Baxter A, Mittler R, Suzuki N (2014) ROS as key players in plant stress signaling. J Exp Bot 65: 1229-1240

Pubmed: Author and Title
CrossRef: Author and Title
Google Scholar: Author Only Title Only Author and Title

Bosch M, Berger S, Schaller A, Stintzi A (2014) Jasmonate-dependent induction of polyphenol oxidase activity in tomato foliage is important for defense against Spodoptera exigua but not against Manduca sexta. BMC Plant Biol 14: 257

Pubmed: Author and Title
CrossRef: Author and Title
Google Scholar: Author Only Title Only Author and Title

Carter C, Healy R, O'Tool NM, Naqvi SMS, Ren G, Park S, et al (2007) Tobacco nectaries express a novel NADPH oxidase implicated in the defense of floral reproductive tissues against microorganisms. Plant Physiol 143: 389-399

Pubmed: Author and Title
CrossRef: Author and Title
Google Scholar: Author Only Title Only Author and Title

Chater C, Peng K, Movahedi M, Dunn JA, Walker HJ, Liang YK, McLachlan DH, Casson S, Isner JC, Wilson I, et al. (2015) Elevated CO2-induced responses in stomata require ABA and ABA signaling. Curr Biol 25: 2709-2716

Pubmed: Author and Title
CrossRef: Author and Title
Google Scholar: Author Only Title Only Author and Title

Cona A, Rea G, Botta M, Corelli F, Federico R, Angelini R (2006) Flavin-containing polyamine oxidase is a hydrogen peroxide source in the oxidative response to the protein phosphatase inhibitor cantharidin in Zea mays L. J Exp Bot. 57 :2277-2289

Pubmed: Author and Title
CrossRef: Author and Title
Google Scholar: Author Only Title Only Author and Title

Cordero OX, Hogeweg P (2006) Feed-forward loop circuits as a side effect of genome evolution. Mol Biol Evol 23: 1931-1936

Pubmed: Author and Title
CrossRef: Author and Title
Google Scholar: Author Only Title Only Author and Title

Desikan R, Cheung MK, Bright J, Henson D, Hancock JT, Neill SJ (2004) ABA, hydrogen peroxide and nitric oxide signaling in stomatal guard cells. Journal of Experimental Botany 55: 205-212

Pubmed: Author and Title
CrossRef: Author and Title
Google Scholar: Author Only Title Only Author and Title

Federico R, Angelini R, Cesta A and Pini C (1985) Determination of diamine oxidase in lentil seedlings by enzymic activity and immunoreactivity. Plant Physiol 79: 62-64

Pubmed: Author and Title
CrossRef: Author and Title
Google Scholar: Author Only Title Only Author and Title

Fincato P, Moschou PN, Ahou A, Angelini R, Roubelakis-Angelakis KA, Federico R, Tavladoraki P (2012) The members of Arabidopsis thaliana PAO gene family exhibit distinct tissue- and organ-specific expression pattern during seedling growth and flower development. Amino Acids 42: 831-841

Pubmed: Author and Title
CrossRef: Author and Title
Google Scholar: Author Only Title Only Author and Title

Foyer CH, Noctor G (2016) Stress-triggered redox signaling: What's in pROSpect? Plant Cell Environm 39: 951-964

Pubmed: Author and Title
CrossRef: Author and Title
Google Scholar: Author Only Title Only Author and Title

Gémes K, Poór P, Horváth E, Kolbert Zs, Szopkó D, Szepesi Á, Tari I (2011) Cross-talk between salicylic acid and NaCl-generated reactive oxygen species and nitric oxide in tomato during acclimation to high salinity. Physiol Plant 142: 179-192

Pubmed: Author and Title
CrossRef: Author and Title
Google Scholar: Author Only Title Only Author and Title

Gilroy S, Suzuki N, Miller G, Choi WG, Toyota M, Devireddy AR, Mittler R (2014) A tidal wave of signals: calcium and ROS at the forefront of rapid systemic signaling. Trends Plant Sci 19: 623-630
Pubmed: Author and Title
CrossRef: Author and Title
Google Scholar: Author Only Title Only Author and Title

Goren R, Palavan N, Flores H, Galston AW (1982) Changes in polyamine titer in etiolated pea seedlings following red light treatment. Plant Cell Physiol 23: 19-26
Pubmed: Author and Title
CrossRef: Author and Title
Google Scholar: Author Only Title Only Author and Title

Graham NA, Tahmasian M, Kohli B, Komisopoulou E, Zhu M, Vivanco I, Teitell MA, Wu H, Ribas A, Lo RS, Mellinghoff IK, Mischel PS, Graeber TG (2012) Glucose deprivation activates a metabolic and signaling amplification loop leading to cell death. Mol Syst Biol 26: 589
Pubmed: Author and Title
CrossRef: Author and Title
Google Scholar: Author Only Title Only Author and Title

Jabs T, Dietrich RA, Dangl JL (1996) Initiation of runaway cell death in an Arabidopsis mutant by extracellular superoxide. Science 273: 1853-1856
Pubmed: Author and Title
CrossRef: Author and Title
Google Scholar: Author Only Title Only Author and Title

Jammes F, Leonhardt N, Tran D, Bousserouel H, Véry AA, Renou JP, Vavasseur A, Kwak JM, Sentenac H, Bouteau F, Leung J (2014) Acetylated 1,3-diaminopropane antagonizes abscisic acid-mediated stomatal closing in Arabidopsis. Plant J 79: 322-333
Pubmed: Author and Title
CrossRef: Author and Title
Google Scholar: Author Only Title Only Author and Title

Ji NR, Park KY (2011) Stress-induced biphasic ethylene and ROS biosynthesis are synergistically interacted in cell damage. J Plant Biotechnol 38:22-29
Pubmed: Author and Title
CrossRef: Author and Title
Google Scholar: Author Only Title Only Author and Title

Kotzabasis K, Christakis-Hampsas MD, and Roubelakis-Angelakis KA (1993) A narrow-Bore HPLC method for the identification and quantification of free, conjugated, and bound polyamines. Analyt Biochem 214: 484-489
Pubmed: Author and Title
CrossRef: Author and Title
Google Scholar: Author Only Title Only Author and Title

Kwak JM, Mori, IC, Pei ZM. Leonhardt N, Torres M, Dangl JL (2003) NADPH oxidase Atrbohd and Atrbohf genes function in ROS-dependent ABA signaling in Arabidopsis. EMBO J 22: 2623-2633
Pubmed: Author and Title
CrossRef: Author and Title
Google Scholar: Author Only Title Only Author and Title

Li L, Li M, Yu L, Zhou Z, Liang X, Liu Z, Cai G, Gao L, Zhang X, Wang Y, Chen S, Zhou JM (2014) The FLS2-associated kinase BIK1 directly phosphorylates the NADPH oxidase RbohD to control plant immunity. Cell Host Microbe 15: 329-338
Pubmed: Author and Title
CrossRef: Author and Title
Google Scholar: Author Only Title Only Author and Title

Maeda H, Yamamoto K, Kohno I, Hafsi L, Itoh N, Nakagawa S, Kanagawa N, Suzuki K, Uno T (2007) Design of a practical fluorescent probe for superoxide based on protection-deprotection chemistry of fluoresceins with benzenesulfonyl protecting groups. Chemistry 3: 1946-1954
Pubmed: Author and Title
CrossRef: Author and Title
Google Scholar: Author Only Title Only Author and Title

Miller G, Suzuki N, Ciftci-Yilmaz S, Mittler R (2010) Reactive oxygen species homeostasis and signaling during drought and salinity stresses. Plant Cell Environ 33: 453-467
Pubmed: Author and Title
CrossRef: Author and Title
Google Scholar: Author Only Title Only Author and Title

Mittler R, Vanderauwera S, Gollery M, Van Breusegem F (2004) Reactive oxygen gene network of plants. Trends Plant Sci 9: 490-498
Pubmed: Author and Title
CrossRef: Author and Title
Google Scholar: Author Only Title Only Author and Title

Moschou PN, Roubelakis-Angelakis KA (2014) Polyamines and programmed cell death. J Exp Bot 65: 1285-1296
Pubmed: Author and Title
CrossRef: Author and Title
Google Scholar: Author Only Title Only Author and Title

Moschou PN, Gutierrez-Beltran E, Bozhkov PV, Smertenko A (2016) Separase Promotes Microtubule Polymerization by Activating

CENP-E-Related Kinesin Kin7. Dev Cell 37: 350-361.
Pubmed: Author and Title
CrossRef: Author and Title
Google Scholar: Author Only Title Only Author and Title

Moschou PN, Delis ID, Paschalidis KA, and Roubelakis-Angelakis KA (2008a) Transgenic tobacco plants overexpressing polyamine oxidase are not able to cope with oxidative burst generated by abiotic factors. Physiol Plant 133: 140-156
Pubmed: Author and Title
CrossRef: Author and Title
Google Scholar: Author Only Title Only Author and Title

Moschou PN, Paschalidis KA, Delis ID, Andriopoulou AH, Lagiotis GD, Yakoumakis DI, and Roubelakis-Angelakis KA (2008b) Spermidine exodus and oxidation in the apoplast induced by abiotic stress is responsible for H2O2 signatures that direct tolerance responses in tobacco. Plant Cell 20: 1708-1724
Pubmed: Author and Title
CrossRef: Author and Title
Google Scholar: Author Only Title Only Author and Title

Moschou PN, Sanmartin M, Andriopoulou AH, Rojo E, Sanchez-Serrano JJ, Roubelakis-Angelakis KA (2008c) Bridging the gap between plant and mammalian polyamine catabolism: a novel peroxisomal polyamine oxidase responsible for a full back-conversion pathway in Arabidopsis. Plant Physiol 147:1845-1857
Pubmed: Author and Title
CrossRef: Author and Title
Google Scholar: Author Only Title Only Author and Title

Moschou PN, Sarris PF, Skandalis N, Andriopoulou AH, Paschalidis KA, Panopoulos NJ, and Roubelakis-Angelakis KA (2009) Engineered polyamine catabolism preinduces tolerance of tobacco to bacteria and oomycetes. Plant Physiol 149: 1970-1981
Pubmed: Author and Title
CrossRef: Author and Title
Google Scholar: Author Only Title Only Author and Title

Moschou PN, Smertenko AP, Minina EA, Fukada K, Savenkov EI, Robert S, Hussey PJ, Bozhkov PV (2013) The caspase-related protease separase (extra spindle poles) regulates cell polarity and cytokinesis in Arabidopsis. Plant Cell 25: 2171-2186
Pubmed: Author and Title
CrossRef: Author and Title
Google Scholar: Author Only Title Only Author and Title

Myhre O, Andersen JM, Aarnes H, Fonnum F (2003) Evaluation of the probes 2',7'-dichlorofluorescin diacetate, luminol, and lucigenin as indicators of reactive species formation. Biochem Pharm 65: 1575-1582
Pubmed: Author and Title
CrossRef: Author and Title
Google Scholar: Author Only Title Only Author and Title

Noctor G, Mhamdi A, Foyer CH (2016) Oxidative stress and antioxidative systems: recipes for successful data collection and interpretation. Plant Cell Environ 39: 1140-1160
Pubmed: Author and Title
CrossRef: Author and Title
Google Scholar: Author Only Title Only Author and Title

Pal M, Szalai G, Janda T (2015) Speculation: Polyamines are important in abiotic stress signaling. Plant Sci 237: 16-23
Pubmed: Author and Title
CrossRef: Author and Title
Google Scholar: Author Only Title Only Author and Title

Papadakis AK, Roubelakis-Angelakis KA (2005) Polyamines inhibit NADPH oxidase-mediated superoxide generation and putrescine prevents programmed cell death induced by polyamine oxidase-generated hydrogen peroxide. Planta 220: 826-837
Pubmed: Author and Title
CrossRef: Author and Title
Google Scholar: Author Only Title Only Author and Title

Paschalidis KA, Tsoumi I, Moschou PN, Roubelakis-Angelakis KA (2010) ABA-dependent amine oxidases-derived H2O2 affects stomata conductance. Plant Signal Behav 5: 1153-1156
Pubmed: Author and Title
CrossRef: Author and Title
Google Scholar: Author Only Title Only Author and Title

Paschalidis KA, Roubelakis-Angelakis KA (2005a) Sites and regulation of polyamine catabolism in the tobacco plant. Correlations with cell division/expansion, cell cycle progression, and vascular development. Plant Physiol 138: 2174-2184
Pubmed: Author and Title
CrossRef: Author and Title
Google Scholar: Author Only Title Only Author and Title

Paschalidis KA, Roubelakis-Angelakis KA (2005b) Spatial and tem- poral distribution of polyamine levels and polyamine anabolism in different organs/tissues of the tobacco plant. Correlations with age, cell division/expansion, and differentiation. Plant Physiol 138: 142-152
Pubmed: Author and Title
CrossRef: Author and Title
Google Scholar: Author Only Title Only Author and Title

Pottosin I, Shabala S (2014) Polyamines control of cation transport across plant membranes: implications for ion homeostasis and

abiotic stress signaling. Front Plant Sci 5: 154
Pubmed: Author and Title
CrossRef: Author and Title
Google Scholar: Author Only Title Only Author and Title

Rodríguez AA, Maiale SJ, Menéndez AB, Ruiz OA (2009) Polyamine oxidase activity contributes to sustain maize leaf elongation under saline stress. J Exp Bot 60: 4249-4262
Pubmed: Author and Title
CrossRef: Author and Title
Google Scholar: Author Only Title Only Author and Title

Sagi M, Fluhr R (2001) Superoxide production by plant homologues of the gp91(phox) NADPH oxidase. Modulation of activity by calcium and by tobacco mosaic virus infection. Plant Physiol 126: 1281-1290
Pubmed: Author and Title
CrossRef: Author and Title
Google Scholar: Author Only Title Only Author and Title

Saha J, Brauer EK, Sengupta A, Popescu SC, Gupta K and Gupta B (2015) Polyamines as redox homeostasis regulators during salt stress in plants. Front Environ Sci 3: 21
Pubmed: Author and Title
CrossRef: Author and Title
Google Scholar: Author Only Title Only Author and Title

Sahebani N, and Hadavi NS (2009) Induction of H2O2 and related enzymes in tomato roots infected with root knot nematode (M. javanica) by several chemical and microbial elicitors. Biocontrol Sci Techn 19: 301-313
Pubmed: Author and Title
CrossRef: Author and Title
Google Scholar: Author Only Title Only Author and Title

Schindelin J, Arganda-Carreras I, Frise E, Kaynig V, Longair M, Pietzsch T, Preibisch S, Rueden C, Saalfeld S, Schmid B, Tinevez JY, White DJ, Hartenstein V, Eliceiri K, Tomancak P, Cardona A (2012) Fiji: an open-source platform for biological-image analysis. Nat Methods 9: 676-682
Pubmed: Author and Title
CrossRef: Author and Title
Google Scholar: Author Only Title Only Author and Title

Snyrychova I, Ayaydin F, Hideg E (2009) Detecting hydrogen peroxide in leaves in vivo - a comparison of methods. Physiol Plantarum 135: 1-18
Pubmed: Author and Title
CrossRef: Author and Title
Google Scholar: Author Only Title Only Author and Title

Song Y, Miao Y, Song CP (2014). Behind the scenes: the roles of reactive oxygen species in guard cells. New Phytol 201: 1121-1140
Pubmed: Author and Title
CrossRef: Author and Title
Google Scholar: Author Only Title Only Author and Title

Suzuki N, Mittler R (2012) Reactive oxygen species-dependent wound responses in animals and plants. Free Rad Biol Medic 53: 2269-2276
Pubmed: Author and Title
CrossRef: Author and Title
Google Scholar: Author Only Title Only Author and Title

Tavladoraki P, Rossi MN, Saccuti G, Perez-Amador MA, Polticelli F, Angelini R, Federico R (2006) Heterologous expression and biochemical characterization of a polyamine oxidase from Arabidopsis involved in polyamine back conversion. Plant Physiol 141: 1519-1532
Pubmed: Author and Title
CrossRef: Author and Title
Google Scholar: Author Only Title Only Author and Title

Tiburcio AF, Altabella T, Bitrián M and Alcázar R (2014) The roles of polyamines during the lifespan of plants: from development to stress. Planta 240: 1-18
Pubmed: Author and Title
CrossRef: Author and Title
Google Scholar: Author Only Title Only Author and Title

Thordal-Christensen H, Zhang Z. Wei Y, Collinge DB (1997) Subcellular localization of H2O2 in plants. H2O2 accumulation in papillae and hypersensitive response during the barley-powdery mildew interaction. Plant J 11: 1187-1194
Pubmed: Author and Title
CrossRef: Author and Title
Google Scholar: Author Only Title Only Author and Title

Torres MA, Dangl JL, Jones JD (2002) Arabidopsis gp91phox homologues AtrbohD and AtrbohF are required for accumulation of reactive oxygen intermediates in the plant defense response. Proc Natl Acad Sci USA 99: 517-522
Pubmed: Author and Title
CrossRef: Author and Title
Google Scholar: Author Only Title Only Author and Title

Wang GF, Li WQ, Li WY, Wu GL, Zhou CY, Chen KM (2013) Characterization of rice NADPH oxidase genes and their expression

under various environmental conditions. J Mol Sci 14: 9440-9458
Pubmed: Author and Title
CrossRef: Author and Title
Google Scholar: Author Only Title Only Author and Title

Wi SJ and Park KY (2002) Antisense expression of carnation cDNA encoding ACC synthase or ACC oxidase enhances polyamine content and abiotic stress tolerance in transgenic tobacco plants. Mol Cells 13: 209-220
Pubmed: Author and Title
CrossRef: Author and Title
Google Scholar: Author Only Title Only Author and Title

Wu JY, Shang ZL, Wu J, Jiang XT, Moschou PN, Sun WD, Roubelakis-Angelakis KA, Zhang SL (2010) Spermidine oxidase-derived H2O2 regulates pollen plasma membrane hyperpolarization-activated Ca2+-permeable channels and pollen tube growth. Plant J 63: 1042-1053
Pubmed: Author and Title
CrossRef: Author and Title
Google Scholar: Author Only Title Only Author and Title

Xue B, Zhang A, Jiang M (2008) Involvement of polyamine oxidase in abscisic acid-induced cytosolic antioxidant defense in leaves of maize. J Integr Plant Biol 51: 225-234
Pubmed: Author and Title
CrossRef: Author and Title
Google Scholar: Author Only Title Only Author and Title

Yun LJ, Chen WL (2006) SA and ROS are involved in methyl salicylate-induced programmed cell death in Arabidopsis thaliana. Plant Cell Rep 30: 1231-1239
Pubmed: Author and Title
CrossRef: Author and Title
Google Scholar: Author Only Title Only Author and Title

Zhang Y, Zhu H, Zhang Q, Li M, Yan M, Wang R, Wang L, Welti R, Zhang W, Wang X (2009) Phospholipase dalpha1 and phosphatidic acid regulate NADPH oxidase activity and production of reactive oxygen species in ABA-mediated stomatal closure in Arabidopsis. Plant Cell 21: 2357-2377
Pubmed: Author and Title
CrossRef: Author and Title
Google Scholar: Author Only Title Only Author and Title

Zhang X, Dong FC, Gao JF, Song CP (2001) Hydrogen peroxide-induced changes in intracellular pH of guard cells precede stomatal closure. Cell Research 11: 37-43
Pubmed: Author and Title
CrossRef: Author and Title
Google Scholar: Author Only Title Only Author and Title

Zhu G, Ding GH, Fang K, Zhao FG, Qin P (2006) New perspective on the mechanism of alleviating salt stress by spermidine in barley seedlings. Plant Growth Regul 49: 147-156
Pubmed: Author and Title
CrossRef: Author and Title
Google Scholar: Author Only Title Only Author and Title